MgF_2-Ta_2O_5 Anti Reflective Coating for 3rd Generation Solar Cells

Dylan J. Mafrici

***Abstract*—A bi-layer anti reflection coating (ARC) composed of MgF_2-Ta_2O_5 was designed using a rigorous mathematical approach and was experimentally tested on a commercial grade solar cell as a proof of concept that the coating can be applied to multi-junction solar cells. A reactive sputter process was used to sputter tantalum oxide and a thermal evaporation process was used for depositing magnesium chloride. The thickness values of each film were measured via profilometry, elipsometry, and reflectometry techniques. Elipsometry was also used to determine the film material's respective index of refraction. Diffuse field reflectance measurements of each film were made using an integrated sphere reflectometer for wavelengths ranging from 400 nm to 700 nm. The ARC was then deposited on a commercial c-Si solar cell (SC) and compared to the same solar cell without the bi-layer ARC. This resulted in a decrease in average reflectivity of 11% on the textured cell surface and an increase in external quantum efficiency (EQE) by 7% for light with wavelengths from 400 nm to 700 nm when the ARC was present.**

***Index Terms*— bi-layer, diffuse reflectance, ARC, EQE, broadband.**

I. Introduction

THE anti-reflective coatings on solar cells play an important role in boosting the devices performance. ARC's have to be carefully designed due to the fact that not all solar cells are created equal. It is well known that a material's band gap ultimately determines the energy of the incoming light that may create an electron-hole pair to generate photocurrent. Third generation solar cells have multiple junctions where cells of different band gap energies are effectively stacked on one another allowing for a wider spectrum of light to be captured. A broadband ARC design can be achieved through mathematically modeling the solar flux as it propagates through to the top of a solar cell. The model can be tested via real life implementation of the necessary processes to deposit such materials being explored.

II. Theory

The way by which the optimum thickness values for the MgF_2-Ta_2O_5 bi-layer were determined was through the method of resultant waves[1]. There are three different sets of equations used to determine the average broadband reflectance (R_{avg}) including the boundary conditions, electric field in *m* dielectric films, and average broadband reflectivity.

Boundary Conditions

$$r_{i-1} = \frac{n_{i-1} - n_i}{n_{i-1} + n_i} \tag{1}$$

$$t_{i-1} = 1 - r_{i-1} \tag{2}$$

$$\delta_i = \frac{2\pi d_i n_i}{\lambda} \tag{3}$$

$$E_+^i = \frac{E_+^{i+1} + r_i E_-^{i+1}}{t_i} \tag{4}$$

$$E_-^i = \frac{r_i E_+^{i+1} + E_-^{i+1}}{t_i} \tag{5}$$

$$n_0|n_1|n_2|n_g = n_{air}|n(\lambda)_{MgF_2}|n(\lambda)_{Ta_2O_5}|n(\lambda)_{Si} \tag{6}$$

Electric Field for m Dielectric Films

$$\boldsymbol{I_i} = \begin{bmatrix} \frac{1}{t_i} & \frac{r_i}{t_i} \\ \frac{r_i}{t_i} & \frac{1}{t_i} \end{bmatrix} \tag{7}$$

$$\boldsymbol{T_i} = \begin{bmatrix} e^{i\delta_i} & 0 \\ 0 & e^{-i\delta_i} \end{bmatrix} \tag{8}$$

$$\boldsymbol{M} = \boldsymbol{I_0} \times \boldsymbol{T_1} \times \boldsymbol{I_1} \times \boldsymbol{T_2} \times \cdots \times \boldsymbol{I_{m-1}} \times \boldsymbol{T_m} \times \boldsymbol{I_m} \tag{9}$$

$$\begin{pmatrix} E_+^0 \\ E_-^0 \end{pmatrix} = \boldsymbol{M} \begin{pmatrix} E_+^f \\ E_-^f \end{pmatrix} \tag{10}$$

$$\begin{pmatrix} E_+^f \\ E_-^f \end{pmatrix} = \begin{pmatrix} 1 \\ 0 \end{pmatrix} \tag{11}$$

Average Broad Band Reflectivity

$$\rho = \frac{E_-^0}{E_+^0} \tag{12}$$

$$R(\lambda) = |\rho||\rho^*| \tag{13}$$

$$R_e = \frac{\int_{\lambda_1}^{\lambda_2} F(\lambda)R(\lambda)d\,\lambda}{\int_{\lambda_1}^{\lambda_2} F(\lambda)d\,\lambda} \tag{14}$$

Where

λ – wavelength (nm)
n – Complex index of refraction as a function of λ
r – Reflectance Fresnel coefficient
t – Transmission Fresnel coefficient
δ – Change in phase of light through a medium
d – Stack layer thickness (nm)
E^+ – Transmitted component of the light's electric field
E^- – Reflected component of the light's electric field
ρ – Stack reflectance coefficient
F – Solar irradiance/flux (photons/m^2s)
R_e – Average stack reflectivity for a range of λ

By utilizing MATLAB, equations 1 through 12 are iteratively ran for varying individual layer thicknesses in a bi-layer ARC. The model is created out of necessity due to the software limitations in PROLITH. A mesh grid of varying layer thicknesses is created and used to make a contour map of the variation of R_{avg}.

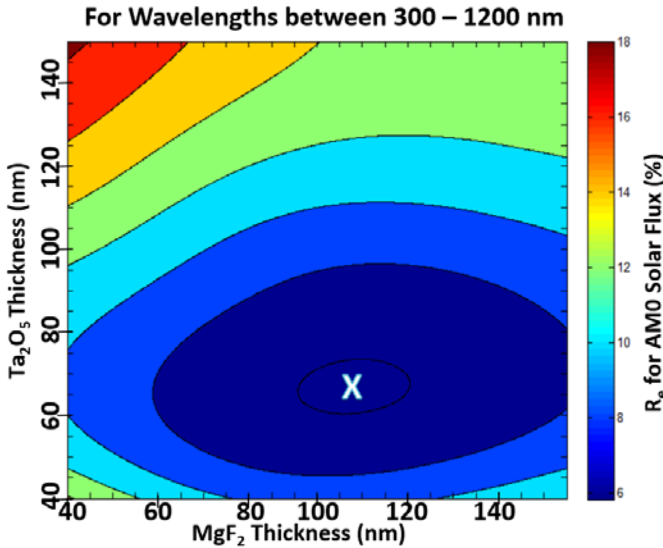

Fig. 1. A contour map where X marks the optimum thickness combination for the bi-layer ARC (105 nm MgF_2 over 70 nm Ta_2O_5).

The resulting simulated reflectance data is imported into PC1D software to see any impacts on a solar cells EQE. The standard PC1D PV cell structure is used to show the affect. In Fig. 2 a notable increase in EQE (~30%) is seen to coincide with the reflectance data generated.

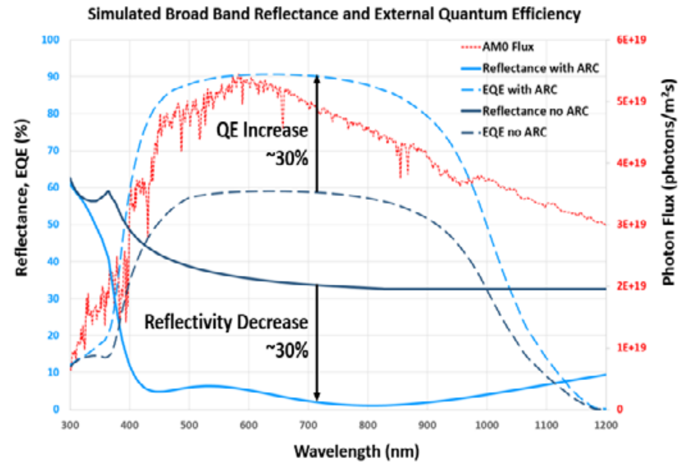

Fig. 2. Bare silicon (dark blue line) reflectance versus when the silicon coated with 105 nm MgF_2 over 70 nm Ta_2O_5 (light blue line) shows the degree by which reflectivity is reduced for AM0 flux from 300 nm to 1200 nm. ARC functionality is shown in PC1D by comparing the quantum efficiencies (blue dotted lines). Red dotted line represents the solar irradiance used in the calculation[2][7][8][4].

Diffuse versus Specular Reflectance

There are multiple ways that reflectance can be measured and some ways are best suited for certain applications, such as solar cell. Specular reflectance only operates on a single light ray at a time so it is hard to get an accurate reflectance measurement on a rough, textured, or patterned surface as the angle of deflection is too much to detect. Diffuse reflectance is all encompassing reflected light from all angles. To get the full picture of the flux of light that is going to waste (i.e reflected), the diffuse reflectance must be taken into consideration.

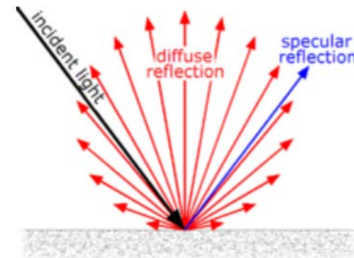

Fig. 3. Diffuse reflection (red) and specular reflection (blue) of the incoming light (black)[5].

III. ARC Deposition Procedure

A. *Commercial ARC Removal*

In order to demonstrate the effect of the MgF_2-Ta_2O_5 bi-layer ARC, a working solar cell was needed due to time constraints that wouldn't allot pv cell processing. Chemical etching of the commercial ARC was done with buffered oxide etch (BOE) and lasted 2.5 hrs due to silicon-nitrides slow etch rate. The crude setup utilized a fluoro-polymer pipe cut by an x-acto knife to fit the solar cell piece. This piper or straw was then left sticking out of a separate small supply of BOE where the cell piece was completely submerged. After bare silicon had be reached and is ready for ARC deposition, the bus bar is masked via a glass

slide in each deposition so that an electrical contact could still be made.

B. Tantalum Oxide Reactive Sputter

The method of deposition for the bottom layer of Ta_2O_5 was chosen to be a reactive sputter process in the SMFL's CVC 601 tool. A 4" 99.999% Ta target was available for use. The inert gas used for ion bombardment was Ar and the reactive gas used was O_2. Eight silicon wafer samples were used in the first design of experiments (DOEs) conducted. Kapton tape was used both as insurance the wafer would remain well placed during processing, and for post deposition step height measurements.

TABLE I. INITIAL CVC601 DOE SETUP

4" Si Wafer	Power (W)	O_2 (mTorr)	Ar (mTorr)	O_2 (%)	Pressure (mTorr)
S5	**300**	**1.5**	**8.5**	**15**	**10**
S4	**300**	**1.5**	**10**	**13**	**11.5**
S8	**300**	**1**	**8.5**	**10.5**	**9.5**
S1	**300**	**1**	**10**	**9.1**	**11**
S6	**350**	**1.5**	**8.5**	**15**	**10**
S3	**350**	**1.5**	**10**	**13**	**11.5**
S7	**350**	**1**	**8.5**	**10.5**	**9.5**
S2	**350**	**1**	**10**	**9.1**	**11**

a. CVC 601 full factorial 2^3 experimental setup. The impacts of DC sputter power, chamber pressure, and oxygen content on the films material properties (index of refraction, deposition rate, surface morphology) are investigated here.

Since the size of the wafer samples used were different than the more common 6" wafers, the platen in the process chamber was swapped out for a platen that accommodated at least eight 4" wafer holders. The choice for symmetry was to use the inner or outer most slots and outermost was chose due to the fact that it was difficult to identify the inner most wafers through the chamber window.

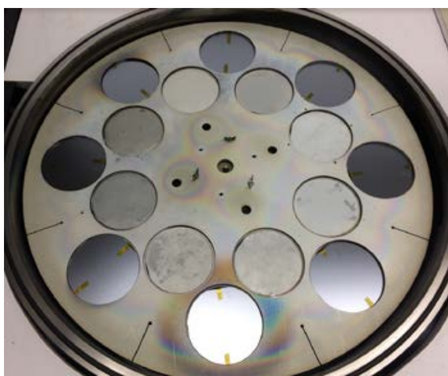

Fig. 4. The 4" platen used in the process chamber of the CVC601 where the silicon wafer samples were numbered clockwise from 1 to 8 (S1 - S8) around the outermost edge.

TABLE II. FIRST RUN DOE RESULTS

4" Si Wafer	Index (n)	Deposition Rate (Å/s)	d_{2ave} (nm)	STD (nm)	STD (%)
S5	**no fit**	**~8**	**46.7**	**7.4**	**15.9**
S4	**no fit**	**~15**	**91.5**	**32.7**	**35.8**
S8	**no fit**	**~22**	**131.8**	**40.5**	**30.7**
S1	**no fit**	**~21**	**127.3**	**26.7**	**21.0**
S6	**no fit**	**~10**	**57.9**	**18.0**	**31.1**
S3	**no fit**	**~31**	**191.6**	**20.2**	**10.6**
S7	**no fit**	**~21**	**129.3**	**41.3**	**32.0**
S2	**no fit**	**~24**	**142.4**	**41.3**	**29.0**

b. CVC 601 full factorial 2^3 experimental setup. The impacts of DC sputter power, chamber pressure, and oxygen content on the films material properties (index of refraction, deposition rate, surface morphology) are investigated here..

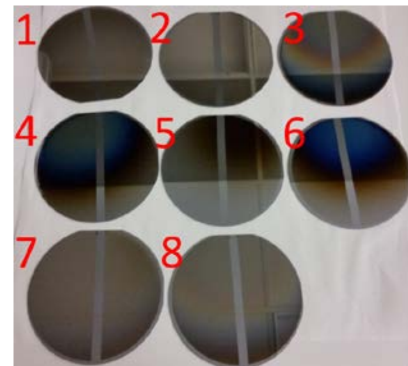

Fig. 5. The numbers 1 – 8 correspond to the S1 – S8 in table b.

Important information was gained from the initial design of experiments regarding sources of film non-uniformities, failure to fit a WVASE model, and the question of deposition power correlating with non-uniformity. The first obvious adjustment is to move to a different platen due to the misalignment between the 4" Ta target and the outer/inner spaces. Another note is that every sample was unable to reliably fit to a Cauchy model and this is believed to be caused by the films light absorption properties. It was suspected that the films may be oxygen deficient, resulting in a more metallic film which have been found to give a more absorbing compound[6]. Upon further investigation with a 4-pt probe, it was found that every sample was ~1000 ohms/square. Another finding was that as power increased, the dep rate did as well but the percent standard deviation (STD) showed little correlation with power.

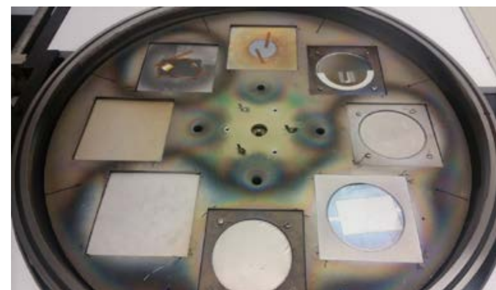

Fig. 6. A square platen that replaced the previous 4" platen in the CVC601. Squares allow for a variety of options for holding different substrates.

TABLE III. FINAL CVC601 DEPOSITION PARAMETERS

Sample	Power (W)	O_2 (mTorr)	Ar (mTorr)	O_2 (%)	Pressure (mTorr)
Clean	400	0	6	0	6
Condition	400	2	4	33	6
S9	400	2	4	33	6
S10	400	2	4	33	6
S13	400	2	4	33	6
S14	400	2	4	33	6
S15	400	2	4	33	6
SC1	400	2	4	33	6

c. CVC 601 final deposition setup part one. These are half of the CVC601 parameters for the final batch of tantalum oxide films after more process knowledge was acquired.

For subsequent Ta_2O_5 reactive sputtering the focus shifted to ensuring that the film contained more oxygen so the largest amount used from the previous DOE was more than doubled such that the gas mixture in the chamber was increased to 33%. To be able to make room for the oxygen, less argon had to be used because the oxygen's pressure contribution was still small even though it's mass flow controller was nearly maxed out at around 96% flow or 9.6 sccm. In addition to this, a square platen replaced the 4" platen so that the substrate-target alignment matches up which will yield better thickness uniformity. A target conditioning step was added after the cleaning step so an oxide could form on the Ta target which can contribute to the films oxygen content when sputtered.

TABLE IV. FINAL REACTIVE SPUTTER RESULTS

Sample	O_2 (sccm)	Ar (sccm)	Time (s)	d_2 P2	(nm) WVASE
S9	8.75/9.08	9/9.5	180	101.3	99.2 ± .5
S10	8.75/9.08	9/9.5	180	95.8	93.5 ± .3
S13	8.67/9.2	9/9.6	180	99.8	98.4± .7
S14	8.87/9.2	9/9.2	126	78.3	80.5 ± .6
S15	8.87/9.2	9/9.2	117	63.6	65.1 ± .2
SC1	8.87/9.2	9/9.2	117	-	-

d. CVC 601 full factorial experimental setup part two. The latter half of the parameters deal with the gas flows and sputter time. The O_2 gas flow was always chosen to be only slightly lower than Ar. Results shown are for profiliometry (P2) and ellipsometry (WVASE).

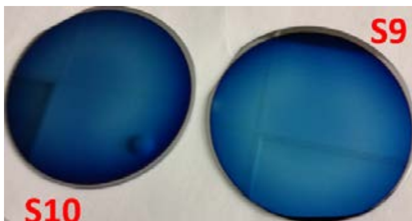

Fig. 7. Snap shot of samples S9 and S10 after removal from the CVC601 process chamber.

After the final depositions are completed, the tantalum oxide seen in Fig. 7 doesn't have trouble fitting to a Cauchy model in the WVASE. The royal blue color is synonymous with highly refractive dielectric materials. The process used to create S9 and S10 was used for all subsequent reactive sputter depositions.

C. Magnesium Fluoride Thermal Evaporation

Since there was an already existing and readily available process known for thermally evaporating MgF_2 in the PVD75A, a DOE was not required. The solar cell piece (SC) was carefully placed on the chuck such that a glass monitor slide masked the metal bus bar thus serving a dual purpose. S15 was used to monitor the ARC thickness and later reflective properties due to the fact that SC has a textured surface.

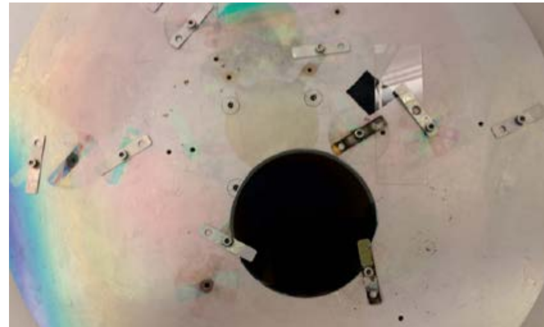

Fig. 8. Sample SC (solar cell) and S15 set up for being loaded in the PVD75A after MgF_2 deposition.

The WVASE is of great use for determining the index of refraction and the experimental measurements from various film depositions show agreement with each other as seen in Fig. 9. This implies that the tantalum-oxide optical properties were not significantly affected by sputter power. Magnesium-fluoride films also showed little variation in index of refraction from sample to sample.

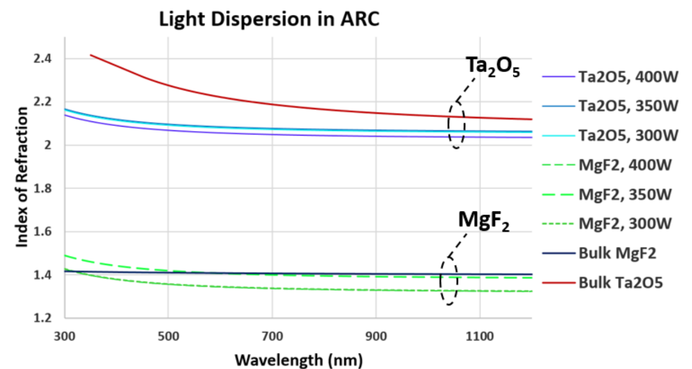

Fig. 9. WVASE results for MgF_2 and Ta_2O_5 layers on silicon substrate for various DC sputter powers[3].

The data gathered in Fig. 9 was imported into the Filmetrics Reflectometer software so that individual and multilayer film stacks of MgF_2- Ta_2O_5 layers were able to be measured. The advantage of this is that it is a much faster way to verify a film's thickness and it can be directly compared to profilometer step height measurements to test for accuracy. An example of this is seen in Fig. 10.

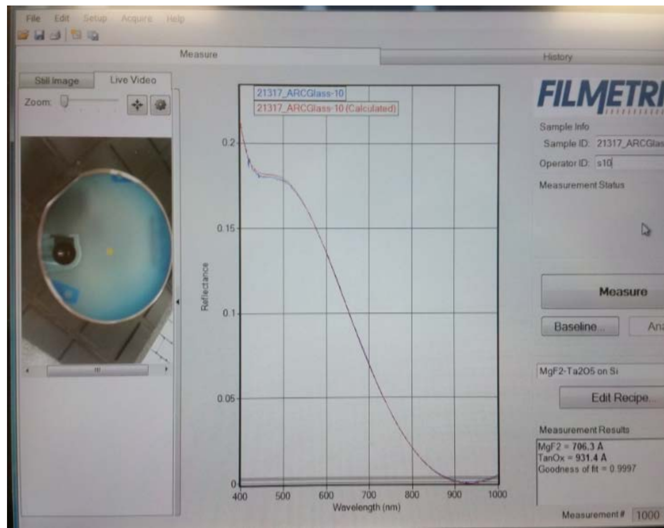

Fig. 10. Filmetrics Reflectometer results for MgF_2 and Ta_2O_5 layers on silicon substrate for S10. The results show 706.3 Å MgF_2 and 931.4 Å Ta_2O_5 with a 0.9997 goodness of fit.

IV. Experimental Results & Analysys

A. Diffuse Field Reflectance Measurements

An integrated sphere reflectometer that captures a diffuse field of reflected light from a surface is preferential when dealing with devices like solar cells because a surface that has texture scatters more light than a planar surface.

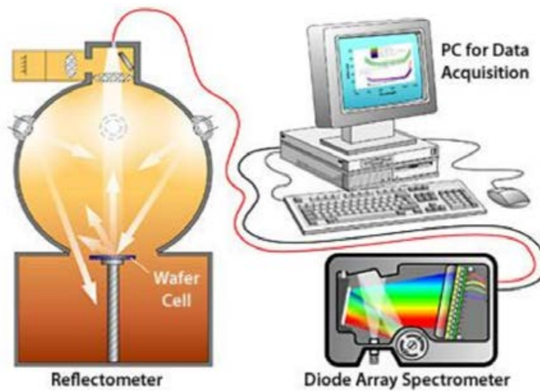

Fig. 11. Diagram of a typical integrated sphere reflectometer where the three main components are the reflectometer itself, a diode array spectrometer, and a computer to store the data[5].

The integrated sphere reflectometer at U of R was able to measure the reflectance of each sample by utilizing a firm foam clamp that presses the sample up against the aperture. Adjusting the aperture to a smaller size allows a smaller area to be taken into account and vice versa with larger apertures. Solar cell pieces are a perfect candidate for the small aperture because the broken cell pieces are relatively small (no bigger than the size of a half dollar coin).

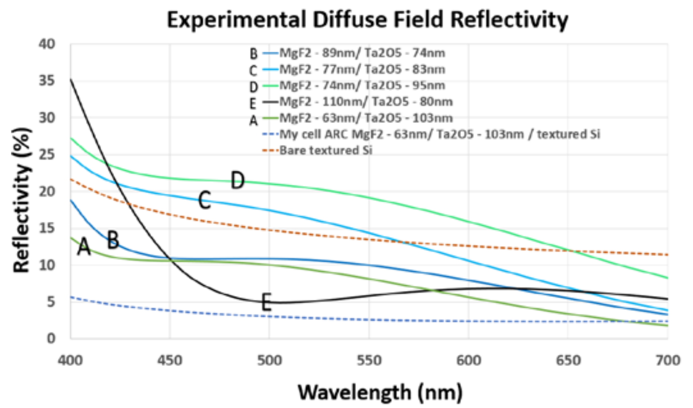

Fig. 12. Diffuse reflectivity measurements of light between 400 nm and 700 nm for film stacks A through E. The dotted lines are texture surfaces, uncoated and coated.

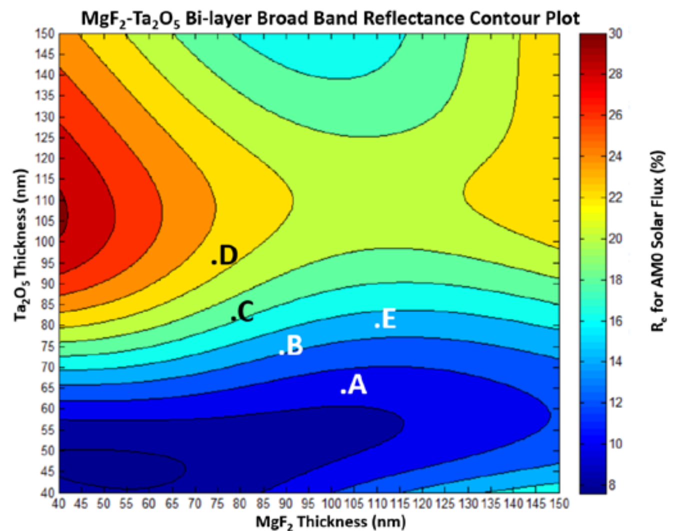

Fig. 13. Contour map of the non-textured films A through E respective average reflectance's where the light range of concern is from 400 nm to 700 nm.

TABLE V. Final Diffuse Reflectance Results

ID (d_1/d_2)	Sim R_{av}(%)	Sim w/Oxide R_{av}(%)	Exp R_{av}(%)
A(103nm-63nm)	**5.5**	**6.0**	**7.2**
B (89nm-74nm)	**6.8**	**9.0**	**8.9**
C (77nm-83nm)	**10.4**	**13.4**	**13.2**
D (74nm-95nm)	**15.0**	**17.6**	**17.4**
E(110nm-80nm)	**6.5**	**8.2**	**8.1**
SC no ARC	**-**	**-**	**14.0**
SC w/ ARC	**-**	**-**	**2.9**

[e.] Diffuse reflectance made at the University of Rochester with the help of the optics department. A corrective oxide interfacial layer brings about better agreement between simulation and results.

Out of each ARC tested, the best porforming ARC was sample A. This correlates directly with the simulation results and the outcomes agree. It should also be noted that when the reflectances are simulated with an interfacial oxide layer, the average reflectivity calculations come fairly close to the experimental. The improvement of reflectivity on a SC is an ~11% decrease as seen in table V.

B. EQE Measurements

There were two solar cell pieces of commercial manufacturer quality measured using the set up seen in Fig. 14. The first point of action that needed to be taken was to get a baseline reading from the silicon reference cell. Once everything is calibrated correctly, the monochromator light beam must be re-focused onto the sample. After the beam is focused on the cell between the grid fingers, the probes should be carefully lowered so as not to disturb the light beam's position on the solar cell. The current pre-amplifier and the digital lock-in amplifier monitor the photocurrent and communicate with a PC to plot the data. An experiments like this should only be conducted when the room is as dark as possible to prevent ambient light from ruining the data.

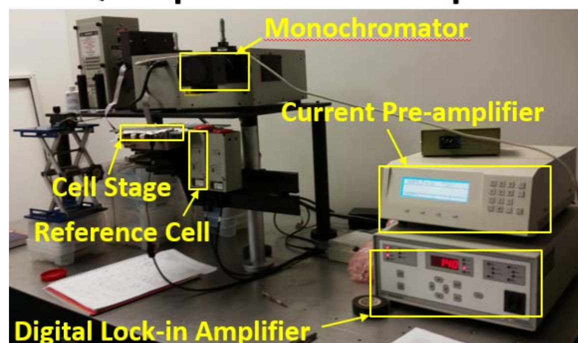

Fig. 14. Set up for measuring quantum efficiency of a solar cell. Not shown here is the computer where the data is graphed and stored

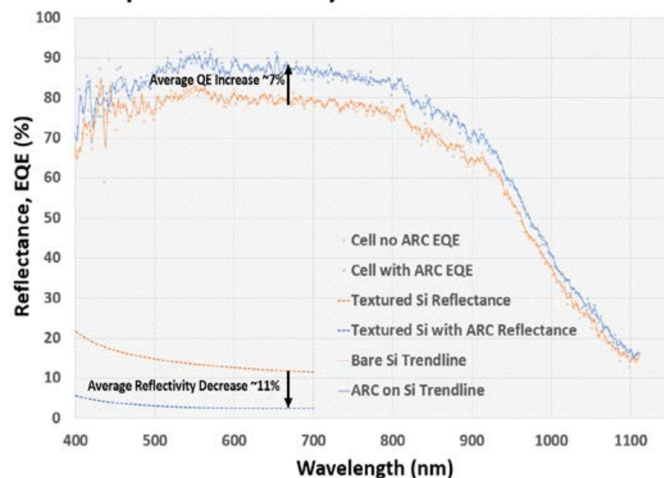

Fig. 15. The SC with the ARC shows an over better quantum efficiency from 400 nm to 1100 nm of light.

The addition of a bi-layer MgF_2-Ta_2O_5 ARC showed a notable improvement in external quantum efficiency for a single junction commercial silicon solar cell with a textured surface. A drop in reflectivity of ~11% corresponded with an increase in external quantum efficiency by ~7% for wavelengths between 400 nm and 700 nm.

V. Conclusion

The optimal thicknesses of the bi-layer materials for the lowest average reflectivity under AM0 spectral irradiance were determined to be 105 nm of MgF_2 on top of 70 nm of Ta_2O_5 through modeling broadband reflectance by applying the method of resultant waves in a MATLAB script. This ARC was successfully deposited with reactive sputter and thermal evaporation techniques using design of experiments to determine the process conditions. The MgF_2-Ta_2O_5 bi-layer ARC resulted in an average reflectivity decrease by 11% and increased the quantum efficiency by 7% in a commercial c-Si solar cell for wavelengths ranging from 400 nm to 700 nm. Although the integrate sphere reflectometer has a more limited measurement range, an improvement in EQE can be seen out to 1100 nm wavelengths which is indicative of a broad band anti-reflective behavior. To show this impact even further, depositing the broad band ARC on a multi-junction solar cell and testing the change in EQE of tandem structure would reveal how it truly effects 3rd generation solar cells.

Acknowledgment

SMFL Staff (special thanks John Nash, Sean O'Brien, and Patrica Meller), University of Rochester, Dr. Jennifer Kruschwitz, NanoPower Research Laboratory, Dr. Seth Hubbard, George MacMurdy, Astha Tapriya, Brittany Smith, Eric Evangelou, Emily Kessler, Jackson Anderson, Dr. Santosh Kurinec, Dr. Rob Pearson, Dr. Dale Ewbank, Dr. Lynn Fuller, Dr. Ivan Puchades, Dr. Michael Jackson

References

[1] Guenther, Robert D. *Modern Optics*. 1st ed. New York, Chichester, Brisbane, Toronto, Singapore: JOHN WILEY & SONS, 1990. Print.

[2] "Quantum Efficiency | Pveducation". *Pveducation.org*. N.p., 2017. Web. 23 Apr. 2017.

[3] "Optical Constants". *RefractiveIndex.info*. N.p., 2008. Web. 23 Apr. 2017.

[4] "Solar Spectral Irradiance: Wehrli 1985 AM0 Spectrum". *Rredc.nrel.gov*. N.p., 1985. Web. 23 Apr. 2017.

[5] "Lecture 23: PV Measurements", Photovoltaic Science & Engineering, S. Kurinec, *Mycourses.rit.edu*, 2017. [Online]. Available: https://mycourses.rit.edu/d2l/le/content/631740/viewContent/4488407/View. [Accessed: 04- May- 2017]

[6] C. Chaneliere, J. Autran, R. Devine and B. Balland, "Tantalum pentoxide (Ta2O5) thin films for advanced dielectric applications", *Materials Science and Engineering: R: Reports*, vol. 22, no. 6, pp. 269-322, 1998 .

[7] "MathWorks - Makers of MATLAB and Simulink", *Mathworks.com*, 2017. [Online]. Available: https://www.mathworks.com/. [Accessed: 18- May- 2017].

[8] PC1D, "PC1D", *SourceForge*, 2017. [Online]. Available: https://sourceforge.net/projects/pc1d/. [Accessed: 18- May- 2017].

[9]" PROLITH Lithography Simulation Tool – Computational Lithography and Photolithography Simulation Tool | KLA-Tencor", *Kla-tencor.com*, 2017. [Online]. Available: https://www.kla-tencor.com/Lithography-Software/chip-prolith.html. [Accessed: 18- May- 2017].

Dylan J. Mafrici is a student at Rochester Institute of Technology in the Department of Electrical and Microelectronic Engineering.